ADVANCING EARTH AND SPACE SCIENCE

Geophysical Research Letters

RESEARCH LETTER
10.1029/2022GL102404

Ice Volume and Insolation Forcing of Abrupt Strengthening of East Asian Winter Monsoon During Glacial Inceptions

Tao Li[1,2], Gaojun Li[2], Tianyu Chen[2], Youbin Sun[3], Qiuzhen Yin[4], Zhipeng Wu[4], Laura F. Robinson[5], Le Li[2], Zeke Zhang[3], Xianqiang Meng[6], Liang Zhao[2], Junfeng Ji[2], and Jun Chen[2]

[1]State Key Laboratory of Palaeobiology and Stratigraphy, Nanjing Institute of Geology and Palaeontology, Chinese Academy of Sciences, Nanjing, China, [2]MOE Key Laboratory of Surficial Geochemistry, Department of Earth and Planetary Sciences, Nanjing University, Nanjing, China, [3]State Key Laboratory of Loess and Quaternary Geology, Institute of Earth Environment, Chinese Academy of Science, Xi'an, China, [4]Georges Lemaître Center for Earth and Climate Research, Earth and Life Institute, Université catholique de Louvain, Louvain-la-Neuve, Belgium, [5]School of Earth Sciences, University of Bristol, Bristol, UK, [6]State Key Laboratory of Lake Science and Environment, Nanjing Institute of Geography and Limnology, Chinese Academy of Sciences, Nanjing, China

Key Points:

- Microcodium $^{87}Sr/^{86}Sr$ record captures the cooling trend in East Asia at the interglacial-glacial transitions
- Decoupled evolution of East Asian winter monsoon and temperature occurred during glacial inceptions
- Ice volume modulates the response of East Asian winter monsoon to insolation-triggered North Atlantic cooling during glacial inceptions

Supporting Information:

Supporting Information may be found in the online version of this article.

Correspondence to:

G. Li,
ligaojun@nju.edu.cn

Citation:

Li, T., Li, G., Chen, T., Sun, Y., Yin, Q., Wu, Z., et al. (2023). Ice volume and insolation forcing of abrupt strengthening of East Asian winter monsoon during glacial inceptions. *Geophysical Research Letters*, *50*, e2022GL102404. https://doi.org/10.1029/2022GL102404

Received 4 DEC 2022
Accepted 24 JAN 2023

Author Contributions:

Conceptualization: Tao Li, Gaojun Li
Funding acquisition: Gaojun Li
Investigation: Tao Li, Gaojun Li
Methodology: Tao Li, Gaojun Li
Validation: Tao Li
Visualization: Tao Li
Writing – original draft: Tao Li, Gaojun Li
Writing – review & editing: Tao Li, Gaojun Li

Abstract It is generally accepted that the glacial-interglacial variations of the East Asian winter monsoon (EAWM) are controlled by the volume of the Northern Hemisphere ice sheets (NHIS), but the fact that they exhibit different evolution patterns during glacial inceptions is often overlooked. By generating an independent chronology framework and integrating multi-proxy records from the loess sections on the central Chinese Loess Plateau, here we show that the rapid intensifying of the EAWM during glacial inceptions reflects millennial perturbations in the large-scale atmospheric circulation in East Asia in response to insolation-triggered abrupt North Atlantic cooling. This climate teleconnection between North Atlantic and East Asia is found to be particularly effective only when the NHIS reaches a critical large size. Our integrated multi-proxy records thus highlight the key role of ice volume in modulating the response of the EAWM to insolation-triggered North Atlantic cooling during the interglacial-glacial transitions.

Plain Language Summary The strength of the East Asian winter monsoon is thought to be dynamically linked to the volume of the Northern Hemisphere ice sheets during the Quaternary glacial-interglacial cycles. Nevertheless, paleoclimatic records generally indicate a rapid shift in the East Asian winter monsoon intensity in the mid-way of the gradual build-up of the Northern Hemisphere ice sheets, meaning that our current understanding of the East Asian winter monsoon dynamics remains elusive. By generating an independent chronology framework and integrating multi-proxy records from the loess sections on the central Chinese Loess Plateau, here we show that the rapid intensifying of the East Asian winter monsoon during glacial inceptions, previously demonstrated as a direct response to the build-up of the Northern Hemisphere ice sheets, actually reflects millennial perturbations in the large-scale atmospheric circulation in East Asia caused by insolation-triggered abrupt North Atlantic cooling when Northern Hemisphere ice sheets reach a critically large size. Our results thus offer new insights into how the climate teleconnections between high- and middle-latitudes of the Northern Hemisphere have controlled the East Asian winter monsoon during glacial inceptions.

1. Introduction

The East Asian winter monsoon (EAWM), a major component of the East Asian monsoon circulation, is characterized by prevailing low-level northwesterly winds tightly linked to the high-northern-latitude climate via the Siberian-Mongolian High (Y. Ding, 1994; Gong et al., 2001) (Figure 1). Our current understanding of the EAWM dynamics during the glacial-interglacial cycles is mostly based on loess records on the Chinese Loess Plateau (CLP) (Liu & Ding, 1998; Xiao et al., 1995), which suggest that the EAWM intensity is closely linked to the volume of the Northern Hemisphere ice sheets (NHIS) on orbital timescale (Ding et al., 1995; Liu & Ding, 1998; Sun et al., 2006). However, unlike the "sawtooth" pattern of global ice volume that shows a gradual build-up of the ice sheets (in ~90,000 years) followed by rapid deglaciation (in ~10,000 years) since the middle Pleistocene transition as documented by the benthic $\delta^{18}O$ records (Lisiecki & Raymo, 2005) (Figure 2a), the loess records of EAWM show distinct glacial and interglacial modes, with the transitions between them generally being quick

10.1029/2022GL102404

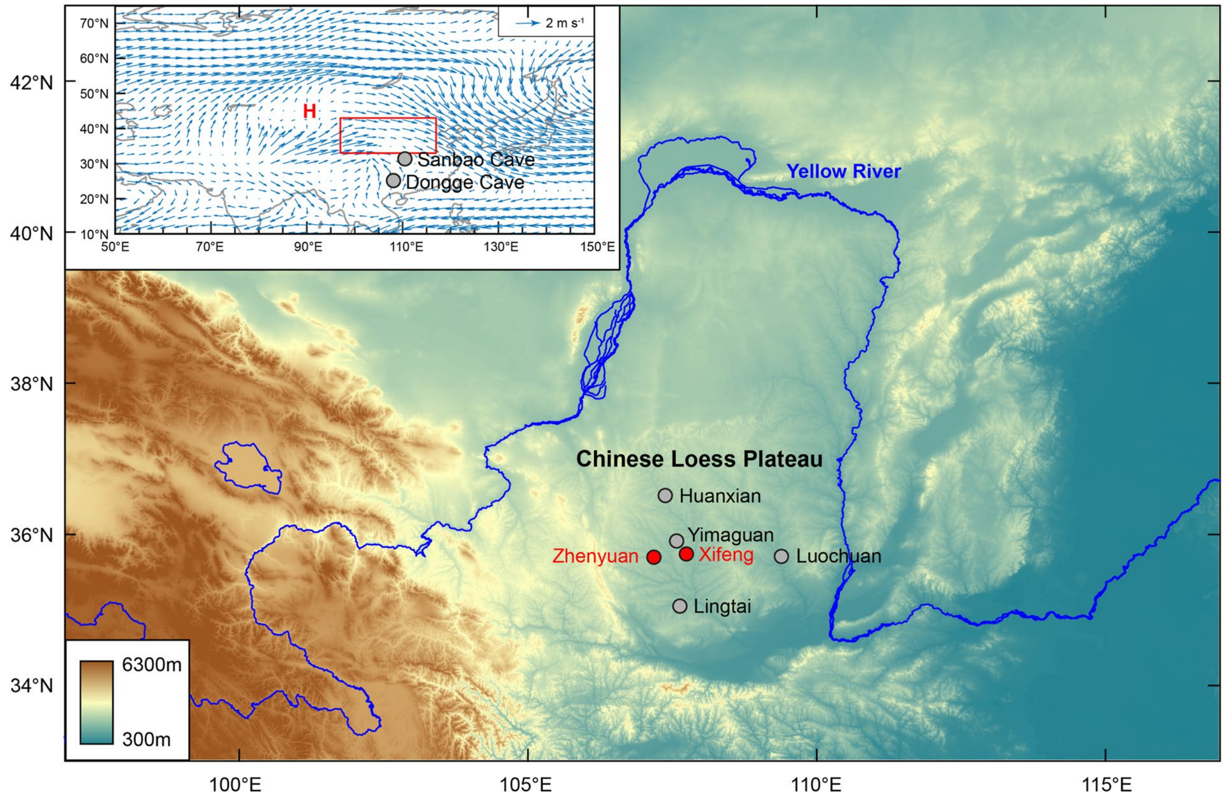

Figure 1. Locations of Xifeng (XF) and Zhenyuan (ZHY) loess profiles on the Chinese Loess Plateau (CLP). Black circles denote four loess profiles investigated in previous studies (Hao et al., 2012; Li et al., 2021; Sun et al., 2010). Red circles represent XF and ZHY loess profiles investigated in this study. Inserted figure in the upper left shows the Dec-Jan-Feb mean surface vector winds based on the NCEP/NCAR Reanalysis data from 1948 to the present at http://psl.noaa.gov/data/gridded/data.ncep.reanalysis.html. H labels the center of Siberian–Mongolian High. The red rectangle refers to the location map. Black circles denote the locations of Sanbao and Dongge caves from the southern China (Cheng et al., 2009, 2016; Wang et al., 2008).

(Figure 2b). This dissimilar evolution pattern between the EAWM and the global ice volume (and NHIS) at the interglacial-glacial transitions means that some key information is missing regarding the dynamics of the EAWM during glacial inceptions (Hao et al., 2012).

The grain size of loess, which is a proxy for the EAWM (Ding et al., 1992, 1995), has been used to establish the chronology framework for the loess deposits by correlating to the benthic $\delta^{18}O$ stack and astronomical tuning (Ding et al., 1994; Sun et al., 2006; Yu & Ding, 1998). Nevertheless, to pinpoint the evolution history of the EAWM and associated climate dynamics during glacial inceptions, it is important to develop an independent age framework for loess deposits that is not tuned based on proxy records related to the EAWM. Magnetic susceptibility (MS) of the loess sequences that accurately traces the loess and paleosol layers, which is regarded as an indicator of the East Asian summer monsoon (EASM) (An et al., 1991), has been used for chronostratigraphy reconstruction (Kukla & An, 1989; Kukla et al., 1988). However, loess MS that reflects the relative amount of magnetic minerals in loess is also modulated by the sedimentation rate and thus EAWM (Kukla et al., 1988). Other proxy records (e.g., Chen et al., 1999; Ding & Yang, 2000; Ding et al., 2001; Liu et al., 2011; Sun et al., 2015, 2019) used to reflect the intensity of pedogenesis (summer monsoon) that show similar patterns to MS are also influenced by the EAWM-controlled deposition rate. Therefore, an independent loess chronology is essential for uncovering the EAWM dynamics during glacial inceptions.

In this article, we present high-resolution secondary carbonate (microcodium) Sr isotope ($^{87}Sr/^{86}Sr$) stratigraphy from two loess-paleosol sequences on the central CLP (Figure 1), yielding an independent chronology framework for assessing the evolution and potential forcing mechanisms of the EAWM during glacial inceptions over the last 550,000 years. Building upon this independent chronology and integrating multi-proxy records, our results offer new insights into the dynamics of the EAWM during glacial inceptions and provide compelling evidence for the millennial-scale teleconnections between the high- and middle-latitudes in terminating the interglacial period in the Northern Hemisphere.

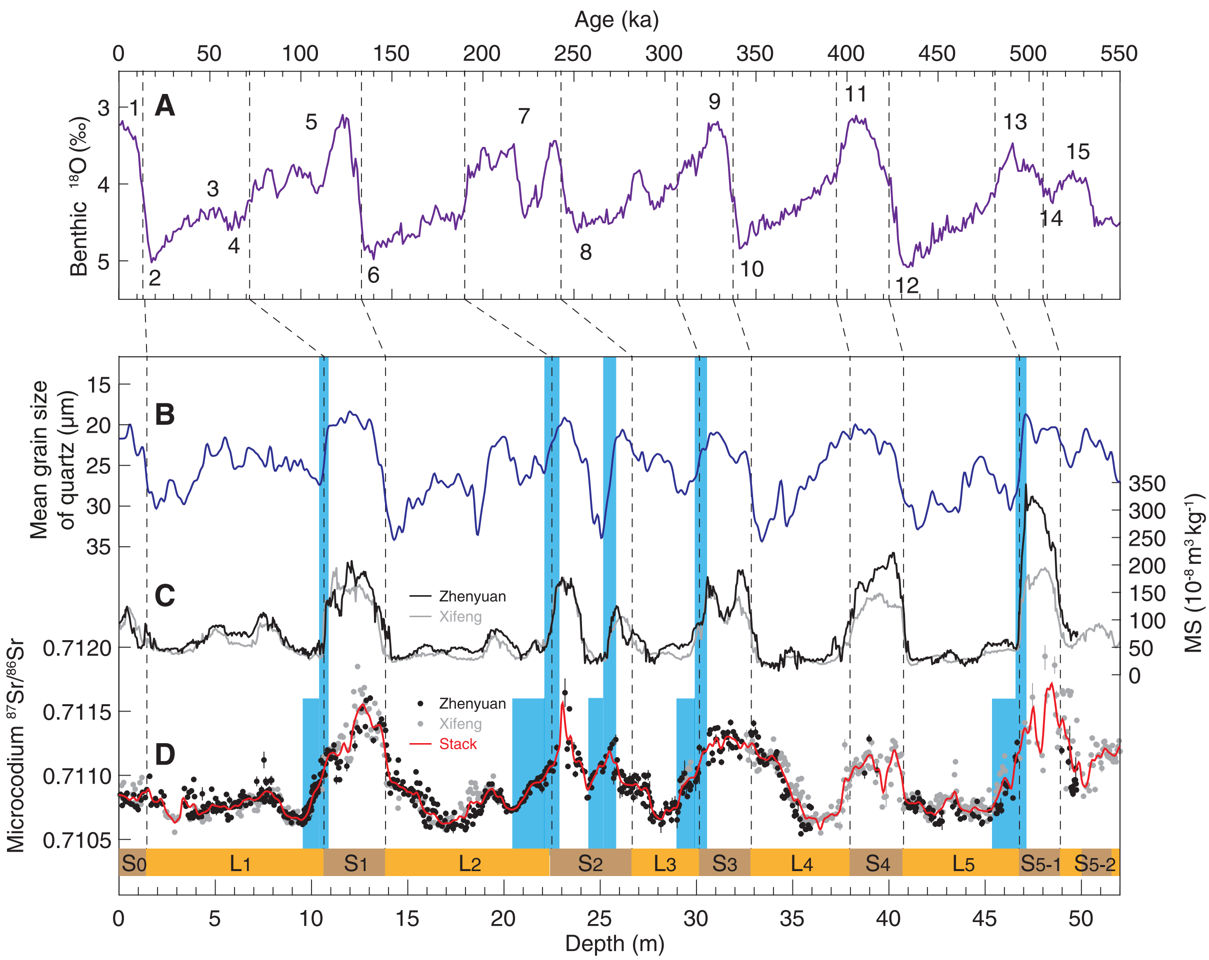

Figure 2. Proxy variations of XF and ZHY loess sequences compared to the LR04 benthic $\delta^{18}O$ stack. (a) LR04 benthic $\delta^{18}O$ stack (Lisiecki & Raymo, 2005). Numbers denote the Marine Isotope Stage (MIS). (b) Mean grain size of quartz (MGSQ) of XF loess (Sun et al., 2006). (c) Magnetic susceptibility (MS) of XF (gray) and ZHY (black) loess profiles. (d) Microcodium $^{87}Sr/^{86}Sr$ records of XF (gray dots) and ZHY (black dots) loess profiles. Error bars denote two standard errors of the mean. The Red line denotes the smoothed microcodium $^{87}Sr/^{86}Sr$ record with a 0.1-m Gaussian filter after aligning ZHY to XF via MS stratigraphy. Vertical dashed lines represent the tie points between the LR04 benthic $\delta^{18}O$ stack and loess sequences previously used for constructing the chronology framework (Sun et al., 2006). Vertical cyan bars denote the concurrent rapid shifts in both MGSQ and MS and prolonged changes in microcodium $^{87}Sr/^{86}Sr$ record at the transition zones between the paleosol layer and the overlying loess layer.

2. Materials and Methods

Two continuous loess-paleosol sequences covering the last six glacial-interglacial cycles (S5 to S0) were collected at Xifeng (XF, 107°47′E, 35°45′N) and Zhenyuan (ZHY, 107°12′E, 35°43′N) on the central CLP (Li et al., 2017) (Figure 1). The loess-paleosol samples were collected every 5 cm in the field, which is equivalent to a typical time resolution of ~500 years. Loess-paleosol sequences at XF and ZHY can be well correlated using MS stratigraphy (Figure S1 in Supporting Information S1). Microcodium tests, which are featured by typical cell-like structure (Li & Li, 2014) (Figure S2 in Supporting Information S1), were hand-picked from the >75 μm fraction under binoscope. The methods of sample preparation and Sr isotope measurement are presented in the Supporting Information S1. The chronology of XF and ZHY sections was established by linking microcodium $^{87}Sr/^{86}Sr$, MS, and mean grain size of quartz (MGSQ) to benthic $\delta^{18}O$ record (Lisiecki & Raymo, 2005) and stalagmite $\delta^{18}O$ record (Cheng et al., 2016) (Figure S3 in Supporting Information S1).

3. Results

The reconstructed microcodium $^{87}Sr/^{86}Sr$ at XF and ZHY varies from ~0.7105 to ~0.712, with higher $^{87}Sr/^{86}Sr$ ratios generally being registered in the paleosol layers compared to the loess layers (Figure 2). Nearly identical microcodium $^{87}Sr/^{86}Sr$ values were observed at the corresponding stratigraphic depths of XF and ZHY. Although microcodium $^{87}Sr/^{86}Sr$, MS, and MGSQ records are characterized by glacial-interglacial variations, they show distinct evolution patterns at the boundaries between the paleosol layers and the overlying loess layers. MS (MGSQ) record generally displays a rapid decreasing (increasing) shift while microcodium $^{87}Sr/^{86}Sr$ record exhibits a gradual, prolonged decreasing trend. Significant positive incursions of microcodium $\delta^{18}O$ and leaf wax δD occurred simultaneously with the rapid shifts in MS (MGSQ) record (Figures 3 and 4). At the boundary between paleosol S4 and loess L4, the decrease of MS occurred synchronously with microcodium $^{87}Sr/^{86}Sr$ and reached a minimum before MGSQ gradually increased (Figure 4).

4. Discussion

4.1. The Temperature-Dependence of Microcodium $^{87}Sr/^{86}Sr$ at XF and ZHY

By generating a high-resolution microcodium $^{87}Sr/^{86}Sr$ record from the paleosol unit S1 (corresponds to Marine Isotope Stage (MIS) 5) at the Huanxian (HX) section (Figures 1 and S4 in Supporting Information S1), Li et al. (2021) suggested that microcodium $^{87}Sr/^{86}Sr$ is primarily controlled by local temperature instead of monsoonal precipitation at HX. The Sr isotopic composition of the soil solution reflects the relative contribution of weathering products of silicate minerals with higher $^{87}Sr/^{86}Sr$ ratios (∼0.7185) (Chen et al., 2007) and of carbonate minerals with lower $^{87}Sr/^{86}Sr$ ratios (∼0.7103) (Rao et al., 2009). Due to the abundant carbonate minerals in loess and strong evapotranspiration on the CLP, the carbonate system in the soil solution is expected to reach saturation quickly after a rainfall event. In this case, a lower temperature would increase the solubility of carbonate minerals and thus promote more contribution of Sr from carbonate minerals (Plummer & Busenberg, 1982). By contrast, the weathering of silicate minerals is positively correlated with temperature following the weathering rate law (Lasaga et al., 1994). As a result, a lower temperature would facilitate more contribution of Sr from carbonate minerals but less contribution of Sr from silicate minerals to the soil solution, and vice versa. Thus, microcodium $^{87}Sr/^{86}Sr$, which records the Sr isotopic composition of the soil solution, may be a proxy for local temperature (Li et al., 2021).

Nevertheless, the temperature dependence of microcodium $^{87}Sr/^{86}Sr$ is likely complicated by two factors when applied to XF and ZHY sections, including varying carbonate contents and mineral sorting effect. Due to the strong downward leaching effect, some paleosol layers are featured by low contents of carbonate minerals in central CLP (Meng et al., 2018) (Figure S5 in Supporting Information S1), meaning that microcodium $^{87}Sr/^{86}Sr$ is predominantly influenced by weathering of silicate minerals with high $^{87}Sr/^{86}Sr$, which differs from the temperature-controlled binary mixing between silicate and carbonate minerals (Li et al., 2021). This is likely supported by the highest microcodium $^{87}Sr/^{86}Sr$ values observed within the paleosol S5 layer where carbonate content is close to zero (Figure S5 in Supporting Information S1). However, the influence of carbonate contents on microcodium $^{87}Sr/^{86}Sr$ is inconsistent with the observations that microcodium $^{87}Sr/^{86}Sr$ is systematically lower at S4 than S1 while carbonate minerals are more abundant at S1 than S4 (Figure S5 in Supporting Information S1). This is likely due to the fact that weathering product $^{87}Sr/^{86}Sr$ is insensitive to varying carbonate abundance when carbonate content reaches a critical level of a few percentages, therefore ruling out the direct influence of carbonate contents on microcodium $^{87}Sr/^{86}Sr$ for most of the samples (except for paleosol S5).

Due to the mineral sorting during eolian transportation, the paleosol layers deposited during the interglacial periods are generally more enriched in fine detrital silicates with high $^{87}Sr/^{86}Sr$ values than the loess layers deposited during the glacial periods (Chen et al., 2007), indicating that the average $^{87}Sr/^{86}Sr$ of detrital silicates is higher in the paleosol layers than the loess layers. This partly accounts for the higher microcodium $^{87}Sr/^{86}Sr$ in the paleosol layers. Because of large uncertainties associated with the $^{87}Sr/^{86}Sr$ values of different size fractions in loess (Chen et al., 2007), the influence of sorting effect on microcodium $^{87}Sr/^{86}Sr$ is difficult to be quantitatively assessed. Nevertheless, there are two main features of microcodium $^{87}Sr/^{86}Sr$ record that cannot be explained by the sorting effect. At the loess/paleosol boundaries (the deglaciations), it is obvious that both microcodium $^{87}Sr/^{86}Sr$ and MGSQ increased before the rapid shifts in MS and MGSQ, especially at the L4/S3 boundary (Figure 2). This increase in microcodium $^{87}Sr/^{86}Sr$ can hardly be attributed to the sorting effect since a coarser grain size is expected to lower the average $^{87}Sr/^{86}Sr$ of detrital silicate. At the transition zones between the paleosol layers and the overlying loess layers, significant part of the decreasing microcodium $^{87}Sr/^{86}Sr$ occurred after the rapid shifts in MS and MGSQ, also indicating controlling factors other than the sorting effect. Because we cannot rule out the possibility of downward migration of microcodium at the loess/paleosol boundaries due to strong summer

10.1029/2022GL102404

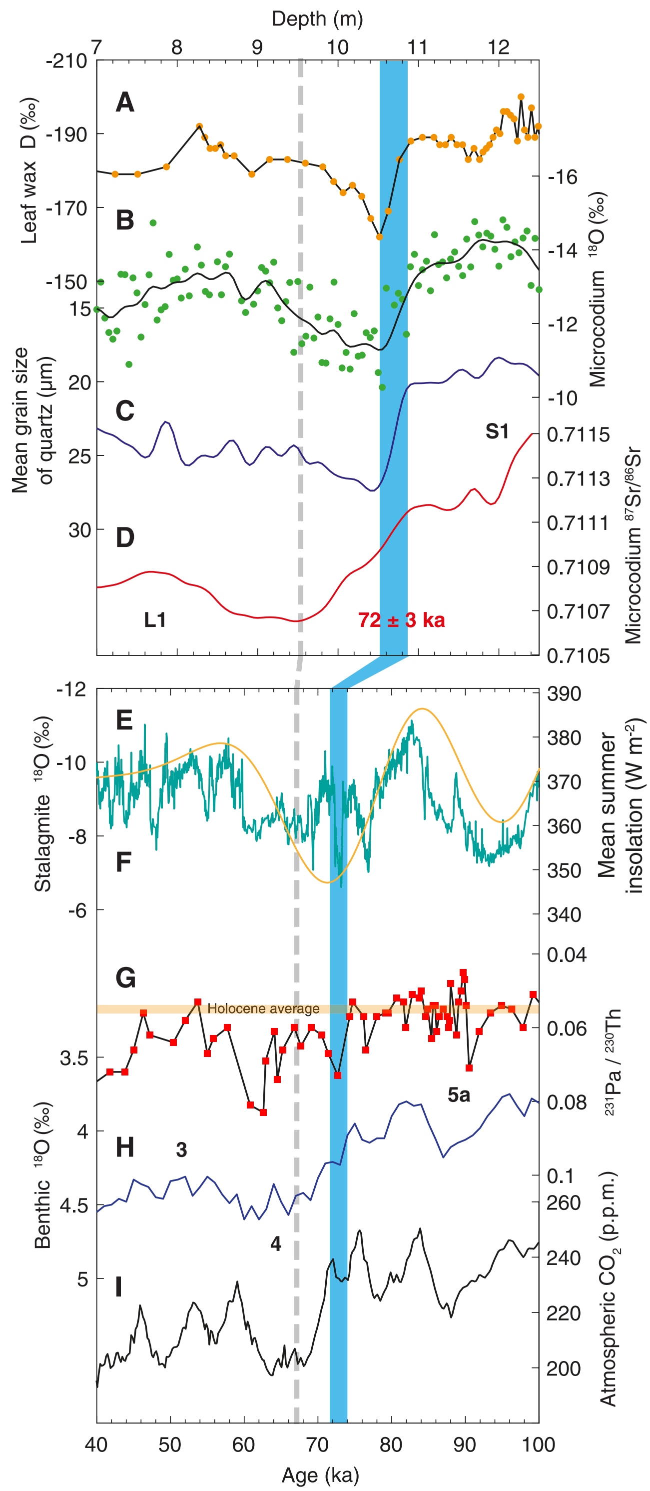

Figure 3. Comparison of proxy records in loess with other paleoclimatic records of the MIS 5a/4 transition. (a) Leaf wax δD record of XF loess (Wang et al., 2021). (b) Microcodium $\delta^{18}O$ record of XF loess (Zhang et al., 2018). (c) MGSQ of XF loess (Sun et al., 2006). (d) Microcodium $^{87}Sr/^{86}Sr$ stack. (e) Asian speleothem $\delta^{18}O$ stack (Cheng et al., 2016). (f) Mean summer (June, July, and August) insolation averaged over 55°N, 65°N, 75°N, and 85°N (Berger, 1978). (g) Bermuda Rise $^{231}Pa/^{230}Th$ record (Bohm et al., 2015). The orange bar denotes the average $^{231}Pa/^{230}Th$ value during Holocene. (h) LR04 benthic $\delta^{18}O$ stack (Lisiecki & Raymo, 2005). (i) The composite atmospheric CO_2 record (Bereiter et al., 2015). The vertical cyan bar and dashed line denote the possible linkage of proxy records in loess and other paleoclimatic records. Note that the absolute age for the S1/L1 boundary determined by the high-resolution luminescence dating of the Luochuan profile is 72 ± 3 ka (Zhang et al., 2022) (Figure 1).

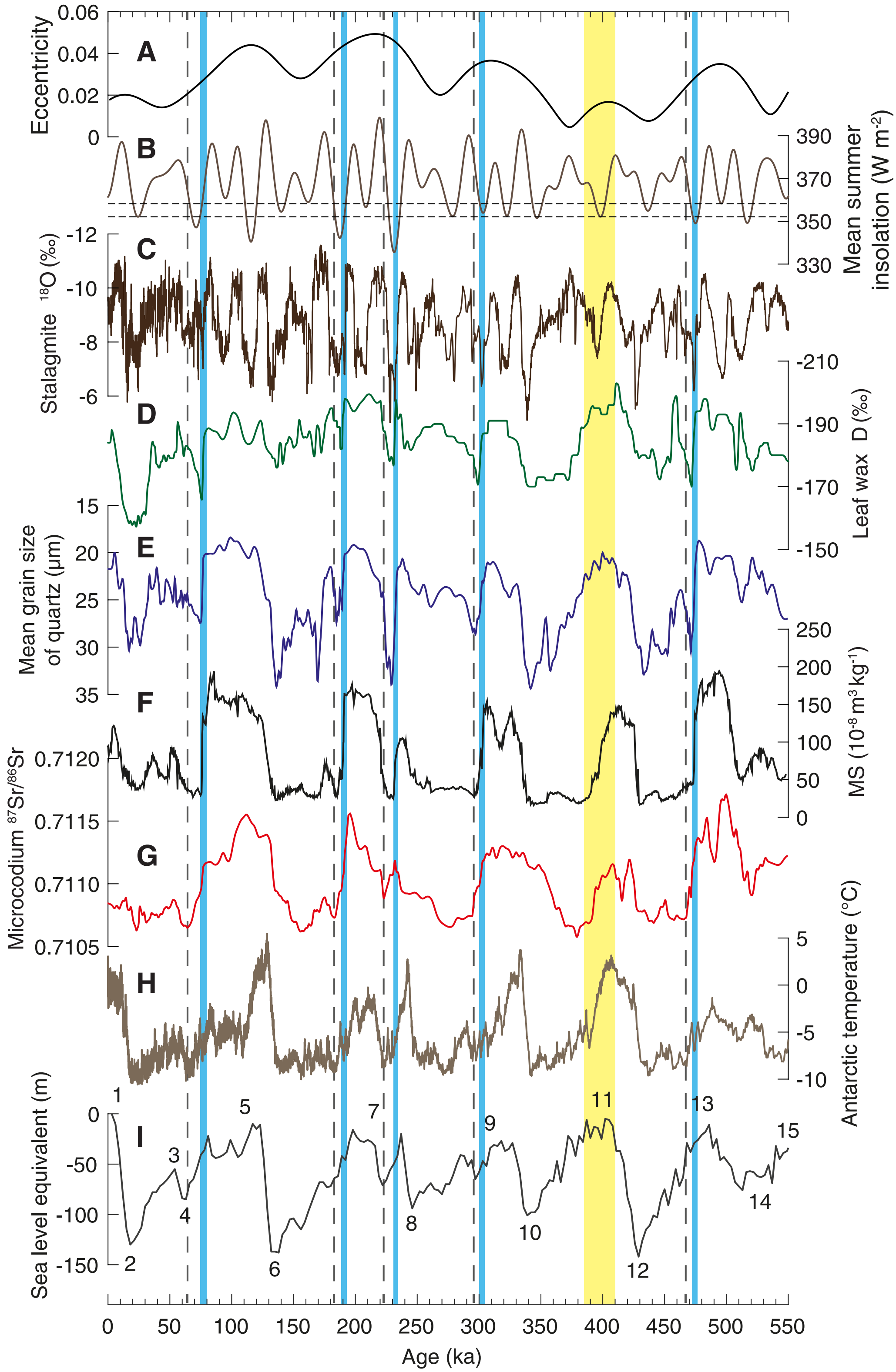
Eccentricity
0.06
0.04
0.02
0
A
B
Mean summer insolation (W m-2)
390
370
350
330
C
Stalagmite 18O (‰)
-12
-10
-8
-6
D
Leaf wax D (‰)
-210
-190
-170
-150
E
Mean grain size of quartz (μm)
15
20
25
30
35
F
MS (10-8 m3 kg-1)
250
200
150
100
50
0
G
Microcodium 87Sr/86Sr
0.7120
0.7115
0.7110
0.7105
H
Antarctic temperature (°C)
5
0
-5
-10
I
Sea level equivalent (m)
0
-50
-100
-150
1
2
3
4
5
6
7
8
9
10
11
12
13
14
15
Age (ka)
0
50
100
150
200
250
300
350
400
450
500
550

Figure 4.

monsoon during the peak interglacials (Meng et al., 2015), we focus on the transition zones between the paleosol layer and the overlying loess layer where the downward migration of microcodium is insignificant.

4.2. Decoupled Evolution of EAWM and Temperature During Glacial Inceptions

The evolution of MS, MGSQ, and microcodium $^{87}Sr/^{86}Sr$ is characterized by a two-stage pattern at the transition zones between the paleosol layers and the overlying loess layers except for the S4/L4 boundary (Figures 2 and S6 in Supporting Information S1). During the first stage, the rapid decrease of MS and the increase of MGSQ occurred simultaneously with the decrease of microcodium $^{87}Sr/^{86}Sr$. This is followed by a relatively stable MS (MGSQ) but continued dropping microcodium $^{87}Sr/^{86}Sr$ to the minimum at the second stage. Although the first stage of decreasing microcodium $^{87}Sr/^{86}Sr$ is partly due to increasing grain size and thus lower average $^{87}Sr/^{86}Sr$ of silicate minerals, this cannot account for the second phase of decreasing microcodium $^{87}Sr/^{86}Sr$ given the relatively constant MGSQ and thus stable mineral sorting. Therefore, the second stage of decreasing microcodium $^{87}Sr/^{86}Sr$ very likely reflects a prolonged cooling trend, suggesting decoupled evolution of the winter monsoon intensity and temperature in East Asia during glacial inceptions. It is worth noting that the evolution of EAWM and temperature also decoupled at the S4/L4 boundary, characterized by delayed intensifying of EAWM compared with glacial cooling (Figure 4).

Compared with the gradual decrease in temperature as shown by the stacked microcodium $^{87}Sr/^{86}Sr$ record, it is obvious that the intensifying of EAWM occurred rapidly at the early stage of glacial inceptions, marked by fast, concurrent shifts in the MS and MGSQ records at the paleosol/loess boundaries (Figure 2). Similar rapid changes in MS and grain size records at the paleosol/loess boundaries have also been documented by other loess-paleosol sequences on the CLP (Hao et al., 2012; Ma et al., 2017) (Figure S7 in Supporting Information S1), suggesting that the abrupt intensifying of EAWM during glacial inceptions is a prevailing phenomenon across East Asia. The decoupled evolution of EAWM and temperature in East Asia is also well-manifested by the high-resolution reconstruction from HX, in which the rapid change in mean grain size at MIS 5a/MIS 4 transition is in sharp contrast to the gradual decrease of microcodium $^{87}Sr/^{86}Sr$ from MIS 5e to MIS 4 although microcodium $^{87}Sr/^{86}Sr$ record is sparse within L1 (Li et al., 2021) (Figure S8 in Supporting Information S1), corroborating the abruptness of the intensifying of EAWM during the course of glacial inceptions.

4.3. Potential Forcing Mechanisms and Implications

Microcodium $\delta^{18}O$ and leaf wax δD records also from XF (Wang et al., 2021; Zhang et al., 2018) are integrated to infer the potential forcing mechanisms of decoupled evolution of EAWM and temperature during glacial inceptions (Figures 3 and 4). Significant positive shifts in microcodium $\delta^{18}O$ and leaf wax δD are observed when rapid increases in MGSQ occurred, which indicates concurrent abrupt changes in the EASM and EAWM (Supporting Information S1). The abrupt shifts in the EASM are also evidenced by the anomalously positive shifts in stalagmite $\delta^{18}O$ during these events (Cheng et al., 2016). Since microcodium $\delta^{18}O$ and $^{87}Sr/^{86}Sr$ are generated from the same archive, the rapid positive incursion of microcodium $\delta^{18}O$ at the first stage of decreasing microcodium $^{87}Sr/^{86}Sr$ lends further support to the abruptness of the EAWM and EASM variations relative to the gradual cooling during glacial inceptions (Figure 3).

The coupled shifts in the EAWM and EASM strongly suggest an impact of the North Atlantic climate on these abrupt changes at the interglacial/glacial transitions. A recent study underscored the key role of local summer insolation in regulating the temperature and sea ice extent at the Northern Hemisphere high-latitudes (Yin & Berger, 2011). During glacial inceptions, it has been shown that the gradual decline of mean summer insolation could reinforce the North Atlantic deep water formation and thus Atlantic meridional overturning circulation (AMOC) via its control on temperature, sea ice extent, and the hydrological cycle in the North Atlantic (Yin et al., 2021). Nevertheless, as mean summer insolation continues to decline and crosses the threshold value, the

Figure 4. Comparison of loess proxy records with other paleoclimatic records over the last 550,000 years (a) Eccentricity (Berger, 1978). (b) Mean summer insolation averaged over 55°N, 65°N, 75°N, and 85°N (Berger, 1978). The horizontal dashed lines denote the upper and lower insolation threshold that may trigger the abrupt weakening of AMOC according to the model simulations (Yin et al., 2021). (c) Asian speleothem $\delta^{18}O$ stack (Cheng et al., 2016). (d) Leaf wax δD record of XF loess (Wang et al., 2021). (e) MGSQ of XF loess (Sun et al., 2006). (f) MS of XF loess. (g) Microcodium $^{87}Sr/^{86}Sr$ stack. (h) Antarctic temperature record (Jouzel et al., 2007). (i) Sea Level Equivalent (SLE) calculated from benthic $\delta^{18}O$ stack after deconvolving the influence of temperature (Shakun et al., 2015). Vetical cyan bars denote the timing of rapid shifts in MS, MGSQ, microcodium $\delta^{18}O$, leaf wax δD, and cave carbonate $\delta^{18}O$. Vertical dashed lines highlight the minima of microcodium $^{87}Sr/^{86}Sr$ at the interglacial/glacial boundaries. The vertical yellow bar highlights the transition between MIS 10 and MIS 11.

10.1029/2022GL102404

expanding sea ice could eventually cover the convection center over the Labrador Sea, leading to an abrupt shutdown of convection (Yin et al., 2021). The abrupt weakening of AMOC would then cause abrupt cooling in the northern North Atlantic, which strengthens the Siberian–Mongolian High cell and thus the EAWM but weakens the EASM (Sun et al., 2012), accounting for the concurrent shifts in MGSQ, microcodium $\delta^{18}O$, and leaf wax δD (Figure 4). This coupled high- and middle-latitude climate shift is also supported by the transient positive incursion of stalagmite $\delta^{18}O$ records from South China (Cheng et al., 2016) and systematic reduction in AMOC strength as documented by the sediment $^{231}Pa/^{230}Th$ record from North Atlantic at the MIS 5a/4 transition (Bohm et al., 2015) (Figure 3).

Nevertheless, the insolation-triggered abrupt weakening of AMOC alone cannot account for the mode shift in the EAWM during glacial inceptions. For example, the $\delta^{18}O$ record from the Iberian Margin and the modeling results both indicate a sharp weakening of AMOC at the MIS 5e/5d transition (Yin et al., 2021) while the loess records show no significant changes in the EAWM from MIS 5e to MIS 5a (Figure 4). One key boundary condition that discriminates the MIS 5a/4 transition from the MIS 5e/5d transition is the size of NHIS, indicating that the gradual build-up of the NHIS during MIS 5 may have played an important role in preconditioning the rapid, coupled shifts in the EAWM and EASM at the MIS 5a/4 transition. This assertion is supported by a modeling study that suggested that large-scale atmospheric circulation in the Northern Hemisphere is only significantly perturbed when NHIS reaches a critically large size (Löfverström et al., 2014). At the MIS 5a/4 transition, the mean summer insolation also crossed the threshold (Yin et al., 2021) (Figure 3), which could trigger an abrupt weakening of AMOC and subsequent strengthening of the EAWM. This effect of insolation could be amplified by the positive ice-temperature feedback due to the larger ice sheets at the MIS 5a/4 transition as compared to the MIS 5e/5d transition. This could explain the large shift of the EAWM at the MIS 5a/4 transition but the insignificant change at the MIS 5e/5d transition. Therefore, we suggest that the gradual declining Northern Hemisphere summer insolation during glacial inceptions may trigger a sudden change in the large-scale atmospheric circulation in East Asia via its effect on the AMOC and North Atlantic climate when NHIS reached a critically large size.

The key role of NHIS in modulating the insolation-triggered abrupt change in the EAWM at the end of interglacial is also well manifested by the transition between MIS 11 and MIS 10 (Figure 4). At the boundary between paleosol S4 and loess L4 (corresponds to the transition between MIS 11 and MIS 10), the decrease of MS occurred synchronously with microcodium $^{87}Sr/^{86}Sr$ and reached a minimum before MGSQ gradually declined, indicating delayed intensifying of EAWM compared to glacial cooling in East Asia at the MIS 11/10 transition. This delayed intensifying of the EAWM has previously been attributed to the delayed build-up of NHIS during the eccentricity minima when the variability of summer insolation is muted (Hao et al., 2012), which is supported by pollen records from southwest Greenland that demonstrate a prolonged "warm" interval during MIS 11 (de Vernal and Hillaire-Marcel, 2008). Delayed ice sheet expansion also seems to be supported by the comparison between the Antarctic temperature record and sea level record, with the former dropping rapidly during MIS 11 and reaching the minimum before the latter begins to decrease (Figure 4). Although model results suggest that insolation-triggered AMOC reduction occurred at the end of MIS 11c (Yin et al., 2021), no concurrent shifts in MGSQ and leaf wax δD are documented at the transition between paleosol S4 and loess L4, indicating the teleconnection between North Atlantic and the CLP is muted at the MIS 11/10 transition due to the limited size of NHIS despite the mean summer insolation crossed the threshold.

5. Concluding Remarks

This study provides new secondary carbonate (microcodium) $^{87}Sr/^{86}Sr$ record and integrates multi-proxy records from the central CLP to reinterpret the response of the EAWM to insolation and ice-sheet forcing during glacial inceptions. Microcodium $^{87}Sr/^{86}Sr$ record, which captures the global cooling trend at the transition zones between the paleosol layer and the overlying loess layer, provides an independent age control for comparing loess records with other paleoclimatic records during glacial inceptions. At the mid-way of glacial cooling, abrupt coarsening occurred synchronously with rapid positive shifts in the hydrogen and oxygen isotopic compositions of precipitation, indicating concurrent abrupt shifts in the EAWM and EASM during glacial inceptions. We suggest that the gradual declining summer insolation in Northern Hemisphere high-latitudes during glacial inceptions may trigger a sudden change in the large-scale atmospheric circulation in East Asia via its effect on the AMOC and North Atlantic climate when NHIS reached a critically large size. The key role of NHIS in modulating the insolation-triggered abrupt changes in the EAWM at the end of interglacial is further supported by the absence of an abrupt shift in the EAWM at the MIS 11/10 transition when the build-up of NHIS delayed due to the eccentricity minima. Our results thus provide compelling evidence for the nonlinear response of the EAWM to ice volume and insolation forcing during the interglacial-glacial transitions.

Data Availability Statement

The data in this study are available in Zenodo (doi: https://doi.org/10.5281/zenodo.7395607).

Acknowledgments

We thank Dr J. Nie and an anonymous reviewer for their constructive comments and W. Zhang and F. Liu for the field assistance. This work was supported by the National Natural Science Foundation of China (41991325, 41877351, 42061130212, 42002198), the Strategic Priority Research Program of the Chinese Academy of Sciences (XDB40010200), and the State Key Laboratory of Palaeobiology and Stratigraphy.

References

An, Z., Kukla, G. J., Porter, S. C., & Xiao, J. (1991). Magnetic susceptibility evidence of monsoon variation on the Loess Plateau of central China during the last 130,000 years. *Quaternary Research*, *36*(1), 29–36. https://doi.org/10.1016/0033-5894(91)90015-w

Bereiter, B., Eggleston, S., Schmitt, J., Nehrbass-Ahles, C., Stocker, T. F., Fischer, H., et al. (2015). Revision of the EPICA Dome C CO_2 record from 800 to 600 kyr before present. *Geophysical Research Letters*, *42*(2), 542–549. https://doi.org/10.1002/2014gl061957

Berger, A. (1978). Long-term variations of caloric insolation resulting from the Earth's orbital elements. *Quaternary Research*, *9*(2), 139–167. https://doi.org/10.1016/0033-5894(78)90064-9

Bohm, E., Lippold, J., Gutjahr, M., Frank, M., Blaser, P., Antz, B., et al. (2015). Strong and deep Atlantic meridional overturning circulation during the last glacial cycle. *Nature*, *517*(7532), 73–76. https://doi.org/10.1038/nature14059

Chen, J., An, Z., & Head, J. (1999). Variation of Rb/Sr ratios in the loess-paleosol sequences of central China during the last 130,000 Years and their implications for monsoon Paleoclimatology. *Quaternary Research*, *51*(3), 215–219. https://doi.org/10.1006/qres.1999.2038

Cheng, H., Edwards, R. L., Broecker, W. S., Denton, G. H., Kong, X., Wang, Y., et al. (2009). Ice age terminations. *Science*, *326*(5950), 248–252. https://doi.org/10.1126/science.1177840

Cheng, H., Edwards, R. L., Sinha, A., Spötl, C., Yi, L., Chen, S., et al. (2016). The Asian monsoon over the past 640,000 years and ice age terminations. *Nature*, *534*(7609), 640–646. https://doi.org/10.1038/nature18591

Chen, J., Li, G., Yang, J., Rao, W., Lu, H., Balsam, W., et al. (2007). Nd and Sr isotopic characteristics of Chinese deserts: Implications for the provenances of Asian dust. *Geochimica et Cosmochimica Acta*, *71*(15), 3904–3914. https://doi.org/10.1016/j.gca.2007.04.033

de Vernal, A., & Hillaire-Marcel, C. (2008). Natural variability of Greenland climate, vegetation, and ice volume during the past million years. *Science*, *320*(5883), 1622–1625. https://doi.org/10.1126/science.1153929

Ding, Y. (1994). *Monsoons over China*. Kluwer Academic Publisher.

Ding, Z., Liu, T., Rutter, N. W., Yu, Z., Guo, Z., & Zhu, R. (1995). Ice-volume forcing of East Asian winter monsoon variations in the past 800,000 years. *Quaternary Research*, *44*(2), 149–159. https://doi.org/10.1006/qres.1995.1059

Ding, Z., Rutter, N., Han, J., & Liu, T. (1992). A coupled environmental system formed at about 2.5 Ma in East Asia. *Palaeogeography, Palaeoclimatology, Palaeoecology*, *94*(1), 223–242. https://doi.org/10.1016/0031-0182(92)90120-t

Ding, Z. L., & Yang, S. L. (2000). C3/C4 vegetation evolution over the last 7.0 Myr in the Chinese Loess Plateau: Evidence from pedogenic carbonate δ13C. *Palaeogeography, Palaeoclimatology, Palaeoecology*, *160*(3–4), 291–299. 3–4. https://doi.org/10.1016/s0031-0182(00)00076-6

Ding, Z. L., Yang, S. L., Sun, J. M., & Liu, T. S. (2001). Iron geochemistry of loess and red clay deposits in the Chinese Loess Plateau and implications for long-term Asian monsoon evolution in the last 7.0 Ma. *Earth and Planetary Science Letters*, *185*(1–2), 99–109. https://doi.org/10.1016/s0012-821x(00)00366-6

Ding, Z., Yu, Z., Rutter, N., & Liu, T. (1994). Towards an orbital time scale for Chinese loess deposits. *Quaternary Science Reviews*, *13*(1), 39–70. https://doi.org/10.1016/0277-3791(94)90124-4

Gong, D.-Y., Wang, S.-W., & Zhu, J.-H. (2001). East Asian winter monsoon and Arctic oscillation. *Geophysical Research Letters*, *28*(10), 2073–2076. https://doi.org/10.1029/2000gl012311

Hao, Q., Wang, L., Oldfield, F., Peng, S., Qin, L., Song, Y., et al. (2012). Delayed build-up of Arctic ice sheets during 400,000-year minima in insolation variability. *Nature*, *490*(7420), 393–396. https://doi.org/10.1038/nature11493

Jouzel, J., Masson-Delmotte, V., Cattani, O., Dreyfus, G., Falourd, S., Hoffmann, G., et al. (2007). Orbital and millennial Antarctic climate variability over the past 800,000 years. *Science*, *317*(5839), 793–796. https://doi.org/10.1126/science.1141038

Kukla, G., & An, Z. (1989). Loess stratigraphy in central China: Palaeogeography, Palaeoclimatology. *Palaeoecology*, *72*, 203–225. https://doi.org/10.1016/0031-0182(89)90143-0

Kukla, G., Heller, F., Liu, X. M., Xu, T. C., Liu, T. S., & An, Z. S. (1988). Pleistocene climates in China dated by magnetic susceptibility. *Geology*, *16*(9), 811–814. https://doi.org/10.1130/0091-7613(1988)016<0811:pcicdb>2.3.co;2

Lasaga, A. C., Soler, J. M., Ganor, J., Burch, T. E., & Nagy, K. L. (1994). Chemical weathering rate laws and global geochemical cycles. *Geochimica et Cosmochimica Acta*, *58*(10), 2361–2386. https://doi.org/10.1016/0016-7037(94)90016-7

Li, T., Hedding, D. W., Chen, J., & Li, G. (2021). Modulation of effective precipitation by temperature in the East Asian monsoon margins during Marine Isotope Stage 5. *Geophysical Research Letters*, *48*(24). https://doi.org/10.1029/2021gl095985

Li, T., & Li, G. (2014). Incorporation of trace metals into microcodium as novel proxies for paleo-precipitation. *Earth and Planetary Science Letters*, *386*, 34–40. https://doi.org/10.1016/j.epsl.2013.10.011

Li, T., Liu, F., Abels, H. A., You, C.-F., Zhang, Z., Chen, J., et al. (2017). Continued obliquity pacing of East Asian summer precipitation after the mid-Pleistocene transition. *Earth and Planetary Science Letters*, *457*, 181–190. https://doi.org/10.1016/j.epsl.2016.09.045

Lisiecki, L. E., & Raymo, M. E. (2005). A Pliocene-Pleistocene stack of 57 globally distributed benthic $\delta^{18}O$ records. *Paleoceanography*, *20*(1). https://doi.org/10.1029/2004pa001071

Liu, T., & Ding, Z. (1998). Chinese Loess and the paleomonsoon. *Annual Review of Earth and Planetary Sciences*, *26*(1), 111–145. https://doi.org/10.1146/annurev.earth.26.1.111

Liu, W., Yang, H., Sun, Y., & Wang, X. (2011). $\delta^{13}C$ values of loess total carbonate: A sensitive proxy for Asian summer monsoon in arid northwestern margin of the Chinese Loess Plateau. *Chemical Geology*, *284*(3–4), 317–322. https://doi.org/10.1016/j.chemgeo.2011.03.011

Löfverström, M., Caballero, R., Nilsson, J., & Kleman, J. (2014). Evolution of the large-scale atmospheric circulation in response to changing ice sheets over the last glacial cycle. *Climate of the Past*, *10*(4), 1453–1471. https://doi.org/10.5194/cp-10-1453-2014

Ma, L., Li, Y., Liu, X., & Sun, Y. (2017). Registration of Precession signal in the last interglacial paleosol (S1) on the Chinese Loess Plateau. *Geochemistry, Geophysics, Geosystems*, *18*(11), 3964–3975. https://doi.org/10.1002/2017gc006964

Meng, X., Liu, L., Balsam, W., Li, S., He, T., Chen, J., & Ji, J. (2015). Dolomite abundance in Chinese loess deposits: A new proxy of monsoon precipitation intensity. *Geophysical Research Letters*, *42*(23), 10391–310398. https://doi.org/10.1002/2015gl066681

Meng, X., Liu, L., Wang, X. T., Balsam, W., Chen, J., & Ji, J. (2018). Mineralogical evidence of reduced East Asian summer monsoon rainfall on the Chinese loess plateau during the early Pleistocene interglacials. *Earth and Planetary Science Letters*, *486*, 61–69. https://doi.org/10.1016/j.epsl.2017.12.048

Plummer, L. N., & Busenberg, E. (1982). The solubilities of calcite, aragonite and vaterite in CO_2-H_2O solutions between 0 and 90°C, and an evaluation of the aqueous model for the system $CaCO_3$-CO_2-H_2O. *Geochimica et Cosmochimica Acta*, *46*(6), 1011–1040. https://doi.org/10.1016/0016-7037(82)90056-4

Rao, W., Chen, J., Yang, J., Ji, J., & Zhang, G. (2009). Sr isotopic and elemental characteristics of calcites in the Chinese deserts: Implications for eolian Sr transport and seawater Sr evolution. *Geochimica et Cosmochimica Acta*, *73*(19), 5600–5618. https://doi.org/10.1016/j.gca.2009.06.028

Shakun, J. D., Lea, D. W., Lisiecki, L. E., & Raymo, M. E. (2015). An 800-kyr record of global surface ocean $\delta^{18}O$ and implications for ice volume-temperature coupling. *Earth and Planetary Science Letters*, *426*, 58–68. https://doi.org/10.1016/j.epsl.2015.05.042

Sun, Y., An, Z., Clemens, S. C., Bloemendal, J., & Vandenberghe, J. (2010). Seven million years of wind and precipitation variability on the Chinese Loess Plateau. *Earth and Planetary Science Letters*, *297*(3–4), 525–535. https://doi.org/10.1016/j.epsl.2010.07.004

Sun, Y., Clemens, S. C., An, Z., & Yu, Z. (2006). Astronomical timescale and palaeoclimatic implication of stacked 3.6-Myr monsoon records from the Chinese Loess Plateau. *Quaternary Science Reviews*, *25*(1–2), 33–48. https://doi.org/10.1016/j.quascirev.2005.07.005

Sun, Y., Clemens, S. C., Morrill, C., Lin, X., Wang, X., & An, Z. (2012). Influence of Atlantic meridional overturning circulation on the East Asian winter monsoon. *Nature Geoscience*, *5*(1), 46–49. https://doi.org/10.1038/ngeo1326

Sun, Y., Kutzbach, J., An, Z., Clemens, S., Liu, Z., Liu, W., et al. (2015). Astronomical and glacial forcing of East Asian summer monsoon variability. *Quaternary Science Reviews*, *115*, 132–142. https://doi.org/10.1016/j.quascirev.2015.03.009

Sun, Y., Yin, Q., Crucifix, M., Clemens, S. C., Araya-Melo, P., Liu, W., et al. (2019). Diverse manifestations of the mid-Pleistocene climate transition. *Nature Communications*, *10*(1), 352. https://doi.org/10.1038/s41467-018-08257-9

Wang, Y., Cheng, H., Edwards, R. L., Kong, X., Shao, X., Chen, S., et al. (2008). Millennial- and orbital-scale changes in the East Asian monsoon over the past 224,000 years. *Nature*, *451*(7182), 1090–1093. https://doi.org/10.1038/nature06692

Wang, Z., Liu, W., Wang, H., Cao, Y., Hu, J., Dong, J., et al. (2021). New chronology of the Chinese loess-paleosol sequence by leaf wax δD records during the past 800 k.y. *Geology*, *49*(7), 847–850. https://doi.org/10.1130/G48833.1

Xiao, J., Porter, S. C., An, Z., Kumai, H., & Yoshikawa, S. (1995). Grain size of quartz as an indicator of winter monsoon strength on the Loess Plateau of central China during the last 130,000 Yr. *Quaternary Research*, *43*(1), 22–29. https://doi.org/10.1006/qres.1995.1003

Yin, Q. Z., & Berger, A. (2011). Individual contribution of insolation and CO_2 to the interglacial climates of the past 800,000 years. *Climate Dynamics*, *38*(3–4), 709–724. https://doi.org/10.1007/s00382-011-1013-5

Yin, Q. Z., Wu, Z. P., Berger, A., Goosse, H., & Hodell, D. (2021). Insolation triggered abrupt weakening of Atlantic circulation at the end of interglacials. *Science*, *373*(6558), 1035–1040. https://doi.org/10.1126/science.abg1737

Yu, Z. W., & Ding, Z. L. (1998). An automatic orbital tuning method for paleoclimate records. *Geophysical Research Letters*, *25*(24), 4525–4528. https://doi.org/10.1029/1998gl900197

Zhang, J., Hao, Q., & Li, S.-H. (2022). An absolutely dated record of climate change over the last three glacial–interglacial cycles from Chinese loess deposits. *Geology*, *50*(10), 1116–1120. https://doi.org/10.1130/g50125.1

Zhang, Z., Li, G., Yan, H., & An, Z. (2018). Microcodium in Chinese loess as a recorder for the oxygen isotopic composition of monsoonal rainwater. *Quaternary International*, *464*, 364–369. https://doi.org/10.1016/j.quaint.2017.10.050

References From the Supporting Information

Dirghangi, S. S., Pagani, M., Hren, M. T., & Tipple, B. J. (2013). Distribution of glycerol dialkyl glycerol tetraethers in soils from two environmental transects in the USA. *Organic Geochemistry*, *59*, 49–60. https://doi.org/10.1016/j.orggeochem.2013.03.009

Eagle, R. A., Risi, C., Mitchell, J. L., Eiler, J. M., Seibt, U., Neelin, J. D., et al. (2013). High regional climate sensitivity over continental China constrained by glacial-recent changes in temperature and the hydrological cycle. *Proceedings of the National Academy of Sciences*, *110*(22), 8813–8818. https://doi.org/10.1073/pnas.1213366110

Guo, B., Nie, J., Stevens, T., Buylaert, J.-P., Peng, T., Xiao, W., et al. (2022). Dominant precessional forcing of the East Asian summer monsoon since 260 ka: Geology. *Geology*, *50*(12), 1372–1376. https://doi.org/10.1130/g50206.1

Kim, S.-T., & O'Neil, J. R. (1997). Equilibrium and nonequilibrium oxygen isotope effects in synthetic carbonates. *Geochimica et Cosmochimica Acta*, *61*(16), 3461–3475. https://doi.org/10.1016/s0016-7037(97)00169-5

Liu, J., Song, X., Yuan, G., Sun, X., & Yang, L. (2014). Stable isotopic compositions of precipitation in China. *Tellus B: Chemical and Physical Meteorology*, *66*(1), 22567. https://doi.org/10.3402/tellusb.v66.22567

Liu, W., & Yang, H. (2008). Multiple controls for the variability of hydrogen isotopic compositions in higher plant n-alkanes from modern ecosystems. *Global Change Biology*, *14*(9), 2166–2177. https://doi.org/10.1111/j.1365-2486.2008.01608.x

Liu, H. C., You, C. F., Huang, K. F., & Chung, C. H. (2012). Precise determination of triple Sr isotopes ($\delta^{87}Sr$ and $\delta^{88}Sr$) using MC-ICP-MS. *Talanta*, *88*, 338–344. https://doi.org/10.1016/j.talanta.2011.10.050

Lu, H., Liu, W., Yang, H., Wang, H., Liu, Z., Leng, Q., et al. (2019). 800-kyr land temperature variations modulated by vegetation changes on Chinese Loess Plateau. *Nature Communications*, *10*(1), 1958. https://doi.org/10.1038/s41467-019-09978-1

Russell, W. A., & Papanastassiou, D. A. (1978). Calcium isotope fractionation in ion-exchange chromatography. *Analytical Chemistry*, *50*(8), 1151–1154. https://doi.org/10.1021/ac50030a036

Xie, S., Pancost, R. D., Chen, L., Evershed, R. P., Yang, H., Zhang, K., et al. (2012). Microbial lipid records of highly alkaline deposits and enhanced aridity associated with significant uplift of the Tibetan Plateau in the Late Miocene. *Geology*, *40*(4), 291–294. https://doi.org/10.1130/g32570.1

Zhang, Z., Li, G., Cai, Y., Cheng, X., Sun, Y., Zhao, J., et al. (2021). Millennial-scale monsoon variability modulated by low-latitude insolation during the last glaciation. *Geophysical Research Letters*, *49*(1). https://doi.org/10.1029/2021gl096773